Bulletin of Electrical Engineering and Informatics
Vol. 15, No. 2, April 2026, pp. 970~985
ISSN: 2302-9285, DOI: 10.11591/eei.v15i2.9763

PSO-tuned bidirectional converter for intelligent electric vehicle charging in vehicle-to-grid and grid-to-vehicle applications

Devarakonda Balasubramanyam, Goda Ganesh Raja Sekhar, Tadanki Vijay Muni
Department of Electrical and Electronics Engineering, Koneru Lakshmaiah Education Foundation, Vaddeswaram, India

Article Info

Article history:

Received Dec 22, 2024
Revised Jan 11, 2026
Accepted Feb 22, 2026

Keywords:

Electric vehicle charging
Power quality
Particle swarm optimization controller
Renewable energy
Smart grid

ABSTRACT

Electric vehicles (EVs) can act as distributed energy storage units in smart grids through vehicle-to-grid (V2G) and grid-to-vehicle (G2V) operations. However, large-scale bidirectional EV charging introduces power quality issues, including harmonic distortion and DC-link voltage fluctuations. This paper presents a PSO-tuned modified dq (MDq) control strategy for a bidirectional EV charging system operating under V2G and G2V modes. A transformer-less bidirectional DC–DC converter and a grid-connected voltage source inverter with an LCL filter are modeled to enable controlled power exchange between the EV battery and the grid. Particle swarm optimization (PSO) is employed to optimally tune the controller gains using a multi-objective fitness function that minimizes grid current harmonics, DC-link voltage error, current ripple, and settling time. Simulation results obtained in MATLAB/Simulink demonstrate that the proposed MDq controller significantly outperforms conventional PI and MDq-PI controllers, achieving a grid current total harmonic distortion (THD) of 2.39% while maintaining stable DC-link voltage and fast dynamic response. The proposed approach enhances power quality, grid stability, and operational reliability, making it suitable for intelligent EV charging in smart grid applications.

Corresponding Author:

Goda Ganesh Raja Sekhar
Department of Electrical and Electronics Engineering, Koneru Lakshmaiah Education Foundation
Green Fields, Vaddeswaram, Guntur, Andhra Pradesh, India
Email: rsgg73@kluniversity.in

1. INTRODUCTION

Future energy generation should employ more renewables and clean vehicles to reduce dependence on conventional fuels due to climate change, pollution, and health risks [1]-[4]. New CO_2 emission-controlling policies have expanded renewable power production and electric vehicle (EV) use in multiple applications. Distribution uses renewable sources like solar and wind. Photovoltaics and wind sources create variable power due to their dynamic input energy. Power imbalances like this can cause grid uncertainty, line congestion, and distribution transformer overload during low power. Due to their slow reaction times, traditional generators cannot handle such sudden power changes. Advanced power electronic battery energy storage system (BESS) interfaces lower net system and operating costs, and provide high rates and fast response times for renewable energy applications. EV batteries can supplement renewable energy sources with smaller batteries to minimize solar power variability [3].

EVs still spend over 95% of their time parked at lunchtime and 50% at home, even though they are becoming more integrated into the distribution grid. A household in a developed country likely has two cars, at least one of which is parked at home. References show that 90% of cars are parked at home for 1/3 of 24 hours. These studies show that EVs drive short distances and park much of the day. This means an EV will likely be parked and plugged in. If left plugged in and grid-connected, EVs can provide vehicle-to-grid

(V2G) and grid-to-vehicle (G2V) services. This method can help distribution system operators (DSOs) save money on BESS purchases and maintenance [4].

Power converter topologies are being designed and built for bidirectional power flow in V2G and G2V applications [5], [6]. With added supplementary loads, this system will maintain vehicle and grid traction. Effectively managing battery bidirectional charging and draining can improve the system for renewable energy sources. While supporting these services, the project's battery system will remain crucial to the power source to improve the solution.

Despite these advances, critical gaps remain in the literature:

- Most existing controllers for bidirectional converters are designed with single-objective metrics or manual tuning, limiting their ability to balance multiple performance criteria such as total harmonic distortion (THD), transient response, and DC-link regulation.
- State-of-the-art optimization techniques are not widely adopted for simultaneous tuning of all key controller gains in the bidirectional EV charging context.
- Prior studies provide limited comparative performance analysis between optimized control strategies and traditional methods under both V2G and G2V operating conditions.
- Few works integrate systematic multi-objective optimization into the controller design for power quality enhancement in grid-connected EV charging systems.

To address these gaps, this paper proposes a particle swarm optimization-tuned modified dq (MDq) control strategy for bidirectional EV charging systems, which uses a multi-objective fitness function to optimally tune controller gains, achieving improved harmonic mitigation, enhanced DC-link voltage stability, reduced current ripple, and accelerated dynamic response.

The rest of the document is organized as, proposed EV fed smart grid system in section 2, while integrated renewables and EVs are among the components of the modern grid that are the subject of section 3's modeling and control. Section 4 delineates the settings and conditions of the simulation along with analysis of the results, and section 5 presents the conclusion.

2. PROPOSED SYSTEM

The purpose of V2G model is to balance peak energy demand and supply while also improving the incorporation of variable renewables into smart grid as shown in Figure 1. V2G, as opposed to typical systems, allows for bidirectional power transmission when charging EV batteries. When parked, an EV or group of EVs can either draw from or deliver power to grid.

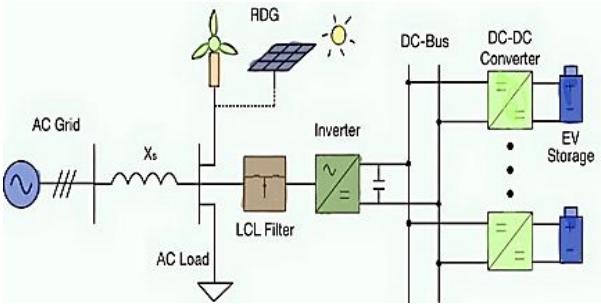

Figure 1. Block diagram of proposed topology

2.1. Electric vehicle battery

An appropriate battery model is required to accurately represent the features of an EV battery. Battery modeling can be approached in three ways: experimentally, electrochemically, and electrically [7]. The electric circuit-based model was adopted for current work due to its ability to precisely reflect the electrical properties of the battery [8]. Figure 2 shows the Shepherd Model, which consists of a regulated voltage source in series with internal resistance. The circuit parameters can be changed to reflect a precise battery model and discharge behavior [9]. A conventional discharge curve is separated into 3 portions, as illustrated in Figure 3.
For the Li type of battery, model utilizes (1)-(4) [10]:
Discharge [$i^*>0$]

$$f_1(it, i^*, i, T, T_a) = E_0(T) - K(T) \cdot \frac{Q(T_a)}{Q(T_a)-it} \cdot (i^* + it) + A \cdot \exp(-B \cdot it) - C \cdot it \quad (1)$$

$$V_{\text{batt}}(T) = f_1(it, i^*, i, T, T_a) - R(T) \cdot i \quad (2)$$

Charge [i^*<0]

$$f_1(it, i^*, i, T, T_a) = E_0(T) - K(T) \cdot \frac{Q(T_a)}{it+0.1)(T_a)} \cdot i^* - K(T) \cdot \frac{Q(T_a)}{Q(T_a)-it} \cdot it + A \cdot \exp(-B \cdot it) - C \cdot it \quad (3)$$

$$V_{\text{batt}}(T) = f_1(it, i^*, i, T, T, T_a) - R(T) \cdot i \quad (4)$$

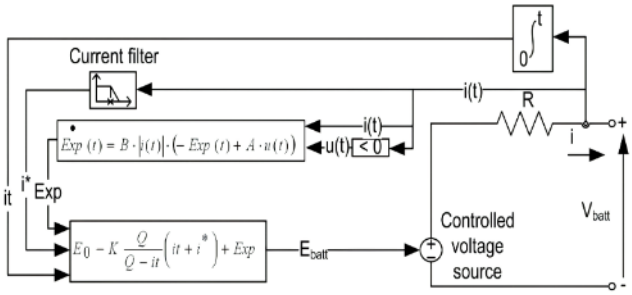

Figure 2. Discharge battery model [4]

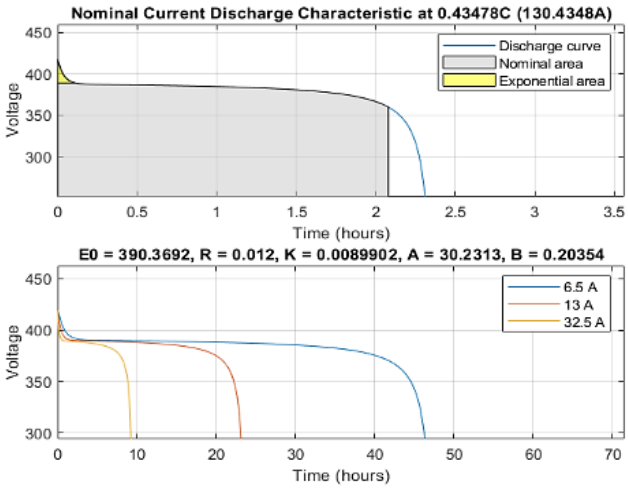

Figure 3. Battery characteristics

2.2. Bidirectional charger

Bidirectional charger model is as shown in Figure 4. The buck/boost topology, as shown in Figure 5, is the most fundamental architecture. However, because there is no electrical separation between the input and output, implementing soft switching might be difficult. Non-isolated converters are often used as interfaces for on-board power sources under DC conversion ratio is minimal, due to their simple design, small size, and high efficiency [11], [12].

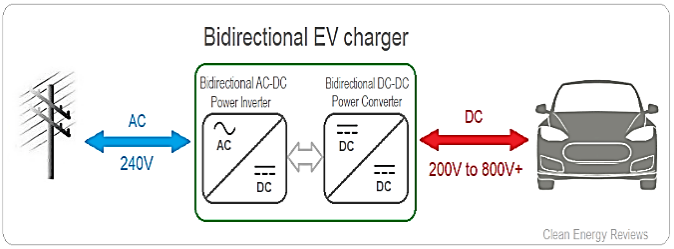

Figure 4. Bidirectional charger

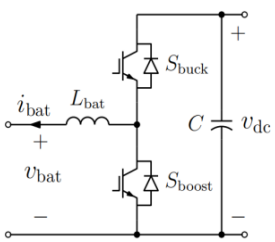

Figure 5. Buck-boost converter

The performance of the battery in the bidirectional charger system is characterized by several key parameters, which define its voltage behavior, capacity, and internal resistance under varying temperature and load conditions. These parameters, along with their typical values, are summarized in Table 1.

Table 1. Battery model parameters

Symbol	Description	Units/typical values
$E_0(T)$	Open-circuit voltage as a function of temperature	Volts (V), 3.6–4.2 V
K(T)	Polarization constant (temperature-dependent)	V/Ah, 0.01–0.1 V/Ah
$Q(T_a)$	Battery capacity at ambient temperature	Ampere-hour (Ah), 10 Ah
it	Extracted/charged capacity	Ah
i*	Filtered current (dynamic current term)	Amperes (A)
i	Instantaneous current	Amperes (A)
R(T)	Internal resistance (temperature-dependent)	Ohms (Ω), 0.2 Ω
A	Exponential zone amplitude	Volts (V), 0.04 V
B	Exponential zone time constant inverse	1/Ah, 3×10^6 1/Ah
C	Linear voltage drop coefficient	Volts/Ah (V/Ah)
T	Battery operating temperature	°C
T_a	Ambient temperature	°C

Figure 6 shows the topology of a 3ϕ VSI. Through the filter, converter is fed to the grid. The ideal AC grid voltages are designated as e_a, e_b, and e_c, and supply currents as i_a, i_b, and i_c. Filter's inductance is represented as L, where R is the resistance. C represents the DC capacitor, whereas u_{dc} and i_{dc} denote the DC voltage and current. DC load is modeled as a series resistance.

The VSI output currents have been corrected using a high-order LCL filter in place of the sophisticated L-filter [4], [8]. In grid-connected inverter systems, passive filters like the L, LC, and LCL filters are employed to reduce harmonic distortion. The grid receives the filtered, harmonic-free current that the LCL filter successfully smooths out of the inverter's output. It provides high harmonic rejection even with modest inductor and capacitor values.

A considerable voltage drop is observed across the L filter [13]. To address this, a high-order LCL filter was used instead of a conventional L-filter to increase the voltage source converter's (VSC) output currents. L filters, LC filters, and LCL filters, are widely used passive filters to minimize harmonics in grid fed inverter systems. The LCL filter is especially successful at smoothing the inverter's current output, sending harmonic-free current to the grid. It achieves excellent harmonic suppression with relatively tiny inductor and capacitor values. The schematic of this filter, showing the inverter-side inductor L_1, grid-side inductor L_2, filter capacitor C_f, damping resistor R_d, and associated currents and voltages, is illustrated in Figure 7.

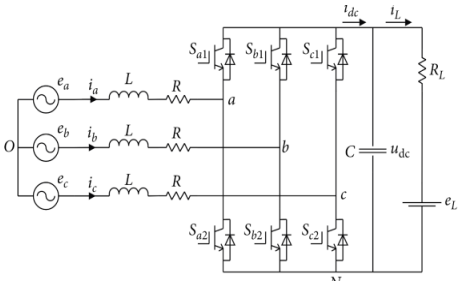

Figure 6. VSC

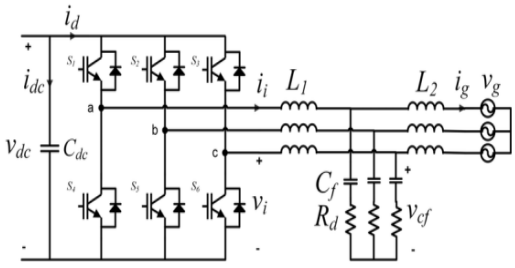

Figure 7. LCL filter

3. CONTROL STRATEGY

3.1. Buck-boost

Serving as a step-down and step-up converter, the buck-boost DC/DC converter may change the input voltage into a lower or higher output voltage. Adjusting the duty cycle allows you to increase or decrease the output voltage.

The structure of the DC-DC converter is shown in Figure 8. In the figure, U_1 and U_2 are the voltage of the low and high voltage terminals of the DC-DC converter (V), I_1 and I_2 are the current of the low and high voltage terminals of the DC-DC converter (A), C_1 and C_2 are the filter capacitor (F), L is the inductor (H), D_1 and D_2 are the diode, S_1 and S_2 are the insulate-gate bipolar transistor (IGBT).

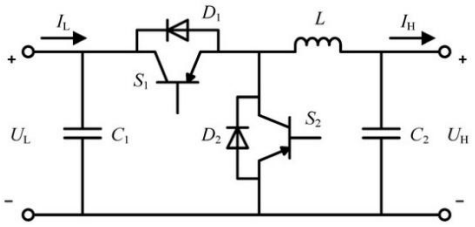

Figure 8. Structure of the DC-DC converter

Figure 9 depicts the current flow throughout the operation. In buck mode presented in Figures 9(a) and (b), assuming the converter operates in continuous conduction, the association between input and output voltages (U_1 and U_2) is provided by $D_{c1}=U_2/U_1$, where D_{c1} denotes duty cycle. The inductor current (i_L) passes left to right. During the interval $0<t\leq D_{c1}T_s$, Q_1 in ON and Q_2 in OFF, leading to a rise in i_L. For $D_{c1}T_s<t\leq T_s$, Q_1 shuts off and Q_2 turns on, leads i_L to reduces. The power passes from source V_1 to the load at V_2 side.

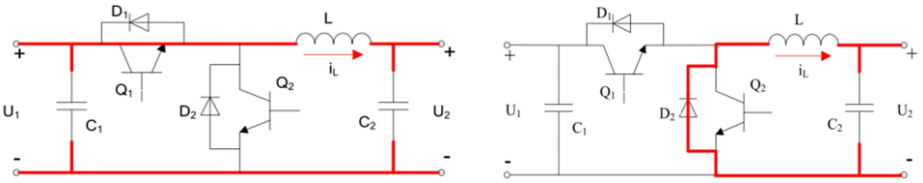

(a) (b)

Figure 9. Buck mode; (a) $0<t\leq D_{c1}T_s$ and (b) $D_{c1}T_s<t\leq T_s$ [14]

Figure 10 depicts the current path throughout the entire operation. As presented in Figures 10(a) and (b) under boost mode, it is also expected that converter runs in continuous conduction mode. The association between input and output voltages (U_1 and U_2) is stated as $U_1/U_2=1/(1-D2)$, where D_{c2} is the duty cycle. Inductor current, i_L, moves from right to left. During the interval $0<t\leq D_{c2}T_s$, Q_1 turns OFF and Q2 turns ON, causing i_L to rise. For $D_{c2}T_s\leq t\leq T_s$, Q_1 turns ON and Q_2 turns OFF, resulting in a drop in i_L. The stored energy in inductor, combined with the DC power from V_2, is delivered to the load on at V_1 side.

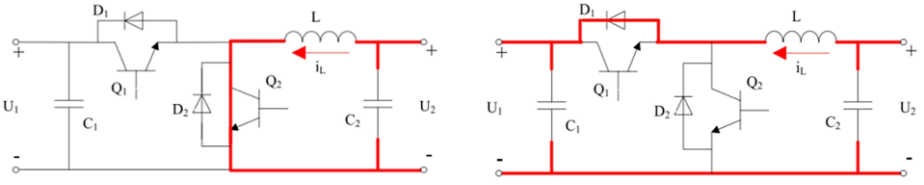

(a) (b)

Figure 10. Boost mode; (a) $0<t\leq D_{c2}T_s$ and (b) $D_{c2}T_s\leq t\leq T_s$

A DC-DC converter can be controlled in two ways: open-loop or closed-loop mode. In the case of a DC battery charger, the input voltage is usually taken as constant [15]. As a result, open-loop control is employed to modulate the terminal voltage applied to the battery by varying the duty cycle. Subsection 3.1 explains the link between terminal voltage (U2) and duty cycle [16].

Table 2 summarizes the operating modes of the proposed converter, detailing the switching intervals, switching conditions, inductor current behavior, voltage relationships, and corresponding power flow characteristics in both buck and boost modes.

3.2. AC-DC converter control

Three-phase converter consist of three source voltage vectors that are spaced 120° apart in phase domain. Voltages are given by (5)-(7):

$$V_a=V_m \cos(\theta_e) \quad (5)$$

$V_b=V_m \cos(\theta_e\text{-}120^\circ)$ (6)

$V_c=V_m \cos(\theta_e\text{-}240^\circ)$ (7)

Table 2. Modes of operation

Mode	Interval	Switching condition	Inductor current behavior	Voltage relationship	Power flow
Buck mode	$0<t\leq Dc_1Ts$	Q_1 ON, Q_2 OFF	Increases (rising)	$Dc_1=U_2/U_1$	Power flows from input source (V_1) to load (V_2)
	$Dc_1Ts<t\leq Ts$	Q_1 OFF, Q_2 ON	Decreases (falling)	$Dc_1=U_2/U_1$	Energy stored in the inductor continues to supply load
Boost mode	$0<t\leq Dc_2Ts$	Q_1 OFF, Q_2 ON	Increases (rising)	$U_1/U_2=1/(1\text{-}Dc_2)$	Energy stored in the inductor builds up
	$Dc_2Ts\leq t\leq Ts$	Q_1 ON, Q_2 OFF	Decreases (falling)	$U_1/U_2=1/(1\text{-}Dc_2)$	Stored energy in inductor and DC power from V_2 supply the load at V_1 side

The conversion from the 3ϕ abc components to the stationary two-phase d-q components is demonstrated using voltage (8)-(10):

$V_a=Ri_a+Ldi_a/dt+Vi_a$ (8)

$V_b=Ri_b+Ldi_b/dt+Vi_b$ (9)

$V_c=Ri_c+Ldi_c/dt+Vi_c$ (10)

In Figure 11 the SRF-PLL, a feedback loop controls the angular position of the dq rotating frame. For small angles between ωt and θ, V_m sin (ωt-θ) can be written as Vm (ωt-θ). When supply voltage is optimally aligned with the d component, the q component of grid voltage becomes zero. The SRF-PLL control loop's large bandwidth allows for quick and accurate detection of grid phase angle when the grid voltage is free of imbalance or harmonics [17]-[20]. However, if the grid voltage is distorted and contains higher-order harmonics, the control loop's bandwidth must be decreased. The most commonly used low-frequency (LF) controller is the PI controller, which functions as a first-order low-pass filter; however, it is not effectively rejects disruptions generated by dominant higher harmonics in a low voltage grid [21]-[25].

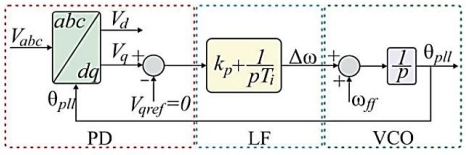

Figure 11. SRF-PLL algorithm

The converter produces an output that is not a perfect sine wave. An LCL filter is designed to minimize current harmonics when power is fed into the grid. If the grid is regarded as an ideal voltage source, the transfer function of the LCL filter is as follows:

$i_g(s)/\ U_i(s)|_{Ug(s)=0}= 1/(L_1L_2C_f)s^3+(L_1+L_2)s$

Numerical coefficients:

$L1\cdot L2\cdot Cf=(5\times10^{-3})(5\times10^{-3})(30\times10^{-6})=7.5\times10^{-10}$
$L1+L2=0.01$

Final numerical transfer function:

$Ig(s)/Ui(s)|Ug(s)=0=1/(7.5\times10^{-10}\ s^3+0.01\ s)=1/[s(7.5\times10^{-10}\ s^2+0.01)]$ (11)

In Figure 12, shunt controller (ShC) with MDq controller is fed. It offsets the demand for reactive power. The ShC in this instance compensates harmonics and reactive component of load current (L1). ShC controls voltage across the DC link as well. The suggested shunt control approach is shown in Figure 5. In this case, load currents were converted to dq0 components provided by (12):

$$I_{Ldq0} = T_s * I_{Labc} \quad (12)$$

where, T_s is transformation matrix

$$T_s = \frac{2}{3}\begin{bmatrix} \text{Cos}[\theta] & \text{Cos}[\theta - 120] & \text{Cos}[\theta + 120] \\ -\text{Sin}[\theta] & -\text{Sin}[\theta - 120] & -\text{Sin}[\theta + 120] \\ 1/2 & 1/2 & 1/2 \end{bmatrix} \quad (13)$$

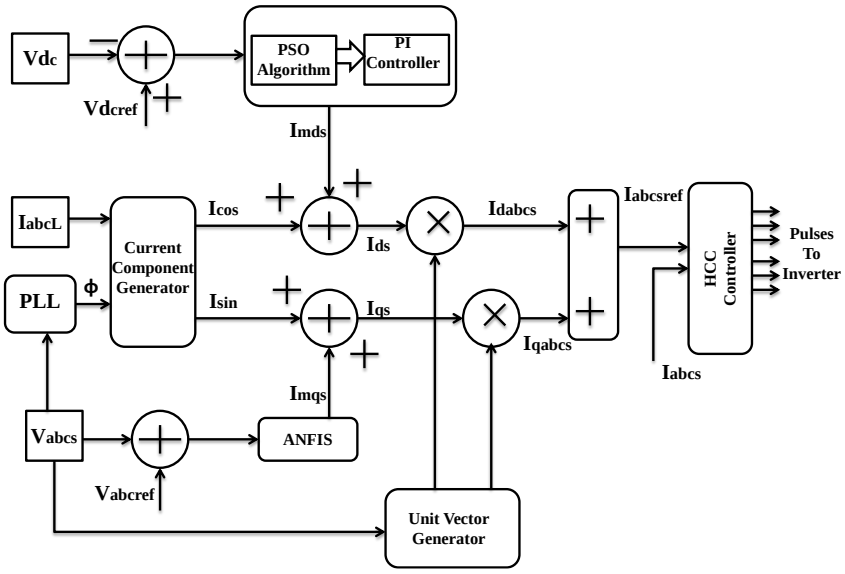

Figure 12. Shunt control with modified Dq- PSO technique [15]

The DC component of I_d is extracted using a low pass filter. In order to stabilize dc link voltage, response of the PI controller is aided with direct axis component of I_L. Reference current's d and q components are thus given by (14) and (15):

$$I_{ref}^{d} = I_{Ld} + \Delta I_{dc} \quad (14)$$

$$I_{ref}^{q} = I_{Lq} \quad (15)$$

Once more, the reference currents' dq0 components are converted into an ABC component frame using (16):

$$I_{ref}^{abc} = T_s^{-1} * I_{ref}^{dq0} \quad (16)$$

For alleviating reactive power and harmonic components in source current, controller gate pulses are produced using hysteresis. The PSO technique is utilized to calculate the PI controller gain values in this model. This approach replaces the conventional PI controller methodology.

3.3. Particle swarm optimization technique

PSO is an evolutionary computation technique that replicates swarm behavior, such as flocks of birds looking for food in a certain area. The PSO algorithm searches the search space for the best solution to a fitness function. It evaluates its success based on each particle's mobility and coordination within the swarm. Each particle moves at random, affected by the swarm's collective experience and its most well-known position. It works toward both the current best global position, Xgb, and its personal best position, Xpb. Figure 13 shows the PSO algorithm that was implemented. The PSO algorithm's fundamental rules are as follows: i) evaluate particle fitness value, ii) update global best position and fitness, and iii) update particle velocity and position.

Let the position vector is $X_i=[x_{i1}, x_{i2,} \ldots x_{in}]$ and velocity vector is $V_i=[v_{i1}, v_{i2,} \ldots v_{in}]$ in search space. Each particle velocity and position are updated using (17) and (18):

$$V_i^{k+1} = w.V_i^k + c_1 .r_1 \left[X_{pb}^k - X_i^k\right] + c_2 .r_2 \left[X_{gb}^k - X_i^k\right] \quad (17)$$

$$X_i^{k+1} = X_i^k + V_i^{k+1} \quad (18)$$

Where I is index of particle, w is the inertia, r_1 and r_2 are random values, c_1 and c_2 are coefficients. The initialization values for PSO algorithm are show in Table 3. Below is the PSO fitness function considered to minimize.

$$J=w_1*THD\_grid+w_2*RMSE(Vdc\_error)+w_3*I\_ripple\_index+w_4*SettlingTime\_index \quad (19)$$

where weights (w1.w4) used in the presented simulations are w1=0.5, w2=0.2, w3=0.2, and w4=0.1.

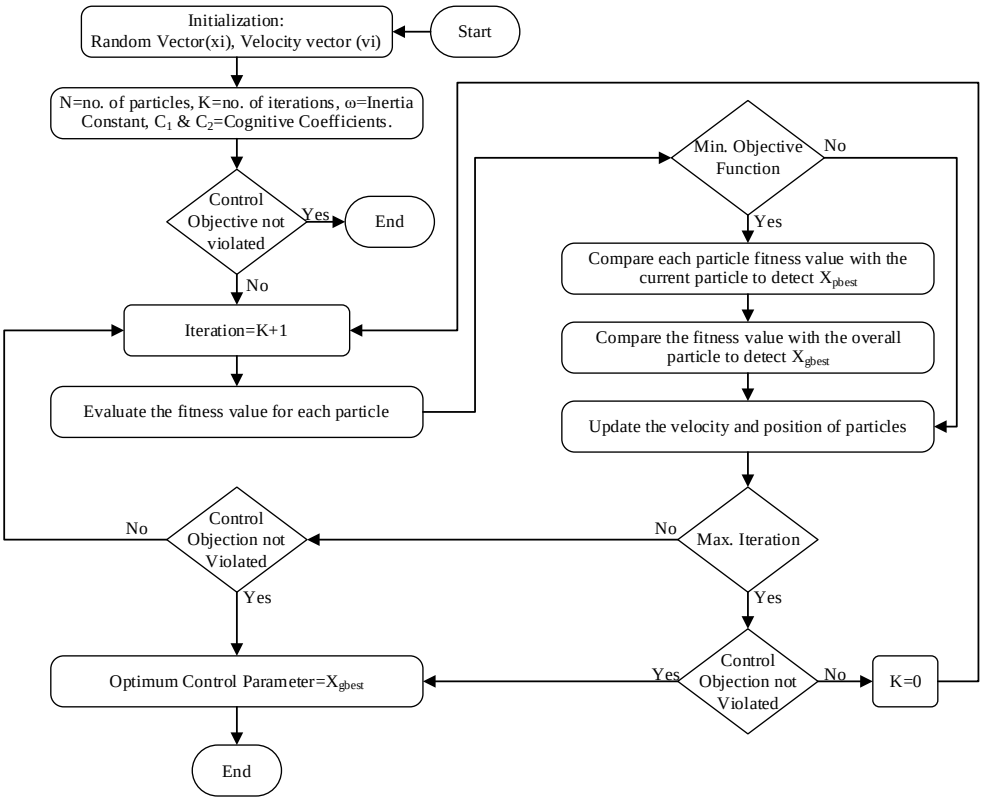

Figure 13. Flowchart of PSO algorithm

The PSO has the following benefits: i) PSO's global search reduces likelihood of local minima in a multi-modal gain landscape, ii) the composite fitness function simultaneously penalizes harmonic content and DC-link deviation, and iii) the MDq-PI structure benefits from PSO's ability to tune multiple interacting gains for both d and q channels.

Table 3. PSO initialization values

Parameter	Value
Inertia, w	0.7
C_1, C_2	1,0
Fitness	1
V_{max}, V_{min}	1,-1
Swarm size	40

4. RESULTS AND DISCUSSION

Table 4 presents the specifications considered for the proposed system modelling, which consists of battery, load, source, DC link voltage, and frequency of switching.

Table 4. PSO initialization values

Circuit element	Parameter	Values
Battery	Nominal voltage	360 V
	Rated capacity	500 Ah
	Initial SoC	50%
	Battery response time	0.9 sec
Load (RL)	Resistance (R)	0.5 mΩ
	Inductance (L)	25 mH
Load (RC)	Resistance (R)	0.5 mΩ
	Capacitance (C)	0.525 mF
3 Phase AC source	Phase voltage	230 Vrms
	Line voltage	415 Vrms
	Frequency	50 Hz
Grid filter	LCL filter (inductance)	5 mH
	Capacitance	30 µF
	Inductance	5 mH
DC link	Capacitor	6600 µF
	Resistor	1.5 mΩ
Switching frequency	For IGBT	15 kHz

4.1. Battery charger simulation

Figure 14 depicts the overall Simulink model of the battery charger, which contains a battery, a constant DC voltage source, and a DC-DC converter. It is vital to remember that UG and LG are PWM control signals for the top and lower MOSFETs, respectively.

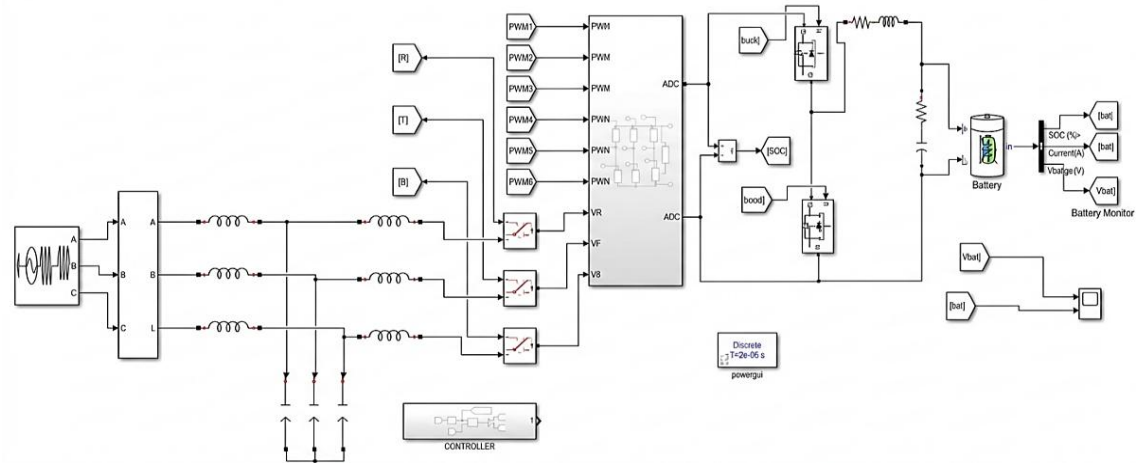

Figure 14. The simulation of the V2G and G2V system

Figure 15 shows that both signals are outputs from the battery controller. The control approach is based on open-loop regulation of the duty cycle, which is achieved by providing a constant voltage reference at the left port of the DC-DC converter that matches to the battery's terminal voltage. If the voltage reference exceeds the battery voltage. When the voltage drops, the battery goes into charging mode, resulting in a negative current value. Conversely, if the voltage reference is lower than the battery voltage, the discharging current is positive. However, if the charger is only used in open-loop mode, the battery may experience troubles where the current surpasses the maximum permitted battery current, IMAX, batt, as shown in Figure 16.

4.2. Vehicle-to-grid and grid-to-vehicle simulation

The control algorithm has been devised to allow for bidirectional power flow. In V2G mode, the vehicle battery discharges to the grid or load. In G2V mode, power is transferred from the grid to the vehicle. In this mode the vehicle charges.

In V2G mode, the PLL algorithm gives critical information on the phase angle of both voltage and current, as well as frequency. This information can be used by modified-DQ control algorithm to deliver power in sync with the grid. Because the VSC output contains current harmonics, an LCL filter is used to smooth the output before it is fed into the grid. Voltage and currents are presented in Figures 17 and 18 depict battery performance, grid three phase current-voltage, in V2G operation.

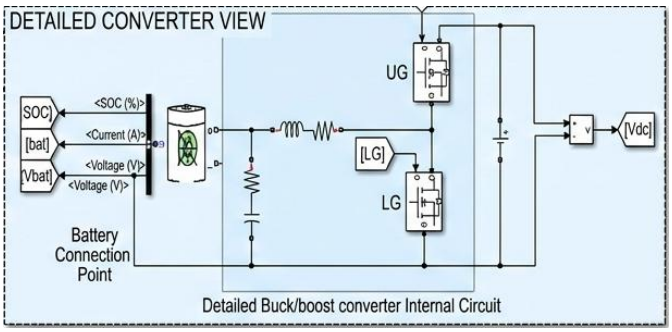

Figure 15. Battery charger simulation

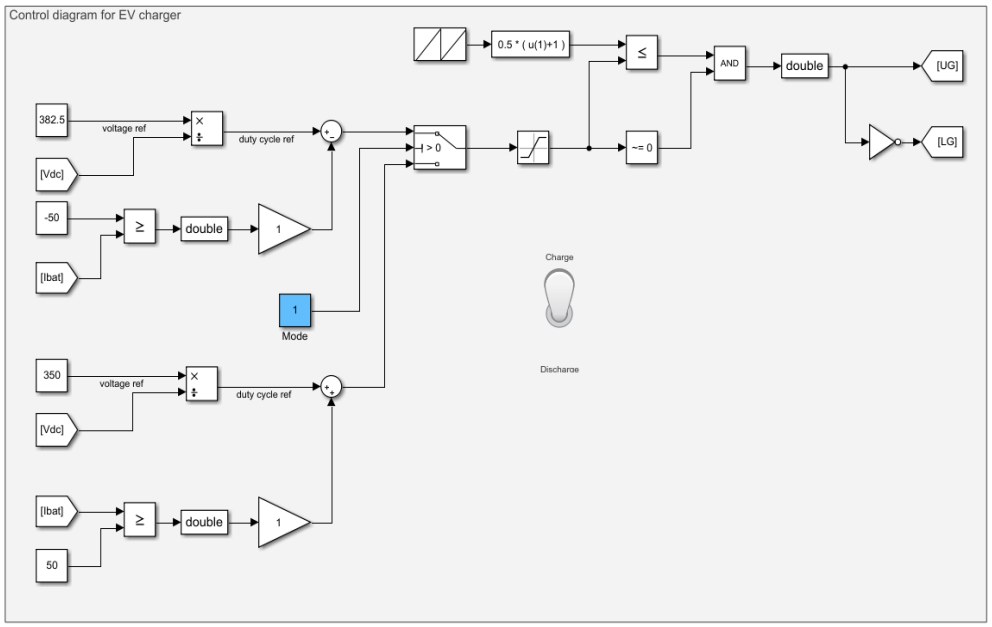

Figure 16. Battery charger controller

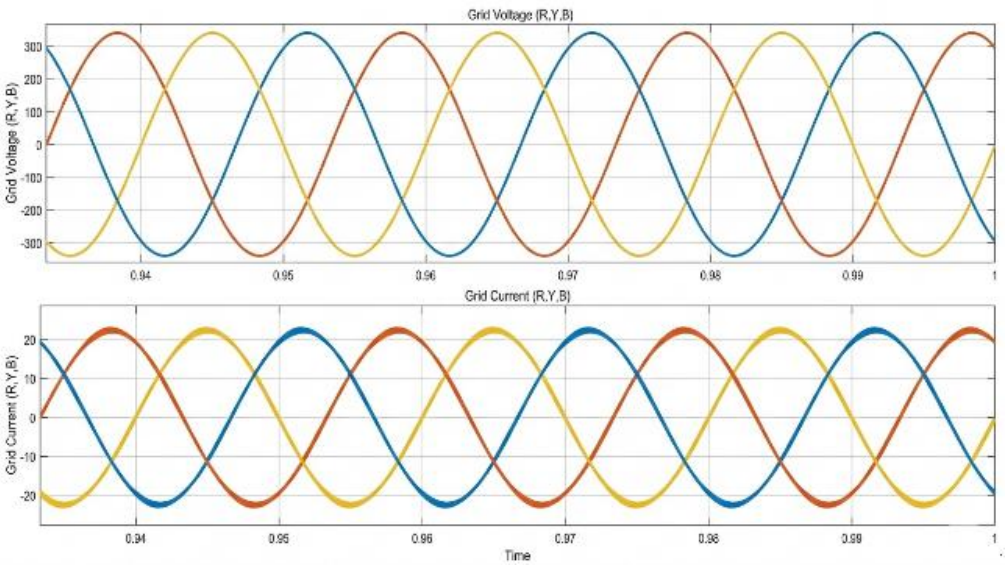

Figure 17. Three phase grid voltages and current in V2G mode

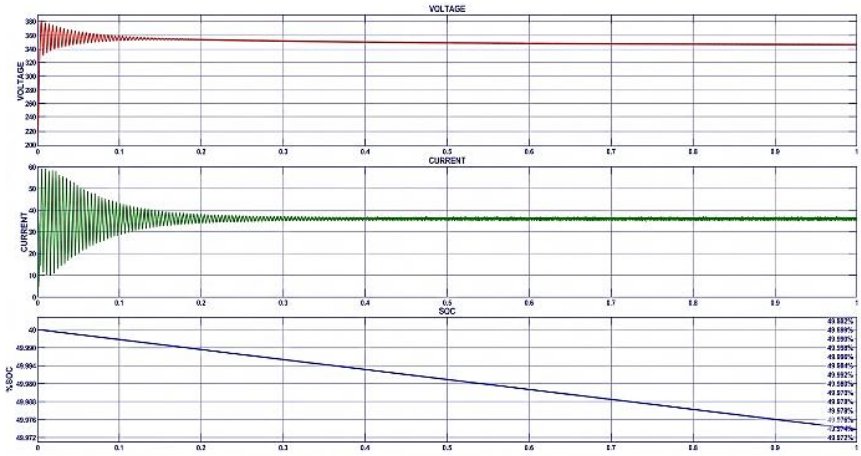

Figure 18. Battery performance in V2G mode

Figure 19 depict DC link voltage and Figure 20 depict under V2G mode, validating the topology's V2G grid operation. This state of zero phase difference indicates that a suitable phase-lock loop is regulated and synchronized. Figure 21 demonstrate battery performance, grid three phase current-voltage, and Figure 22 DC-link voltage accordingly in G2V operation. Figure 23 shows that the grid voltage and current waveforms are 180^0 degrees out of phase, indicating that the topology's G2V grid operation is correct.

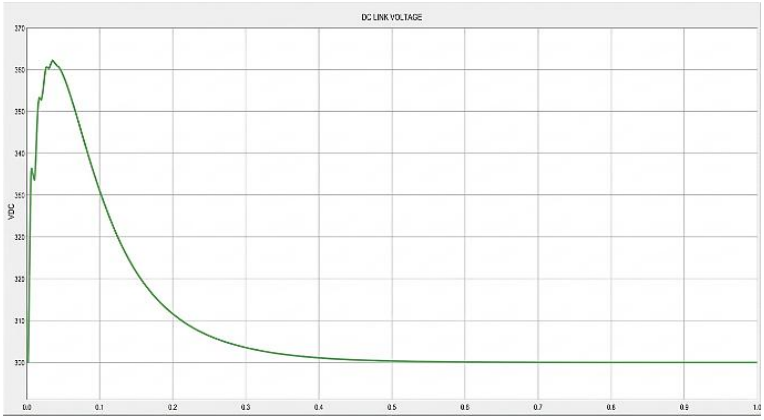

Figure 19. DC link voltage in V2G mode

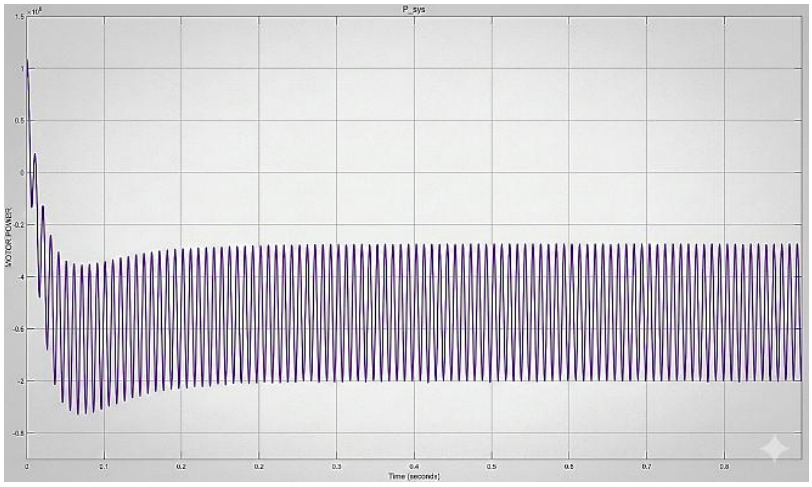

Figure 20. Real power in V2G mode

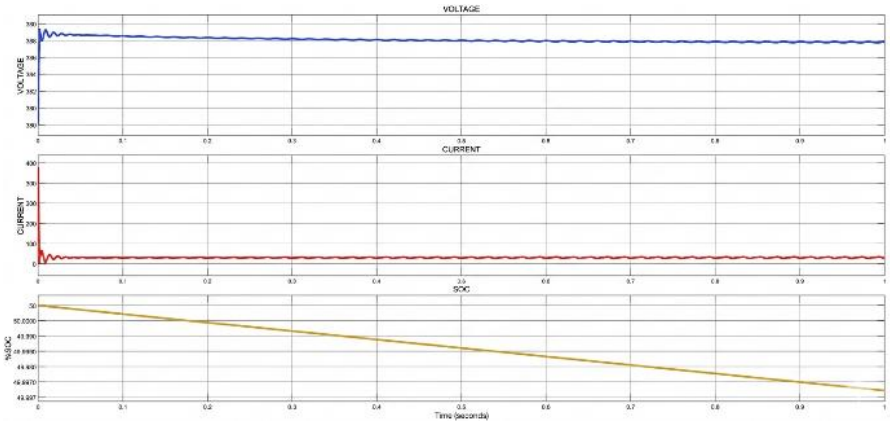

Figure 21. Battery performance in G2V mode

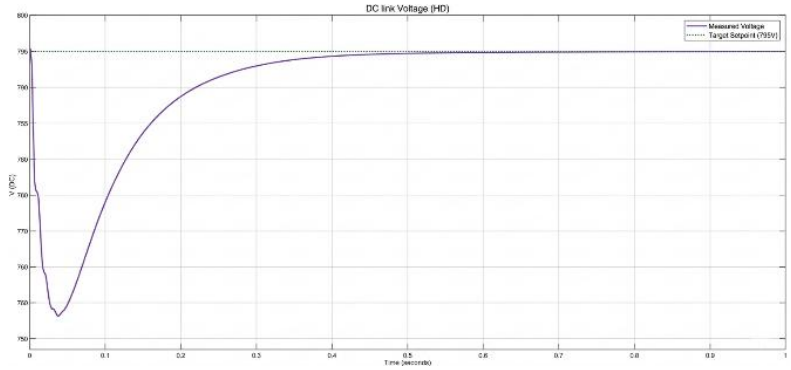

Figure 22. DC link voltage in G2V mode

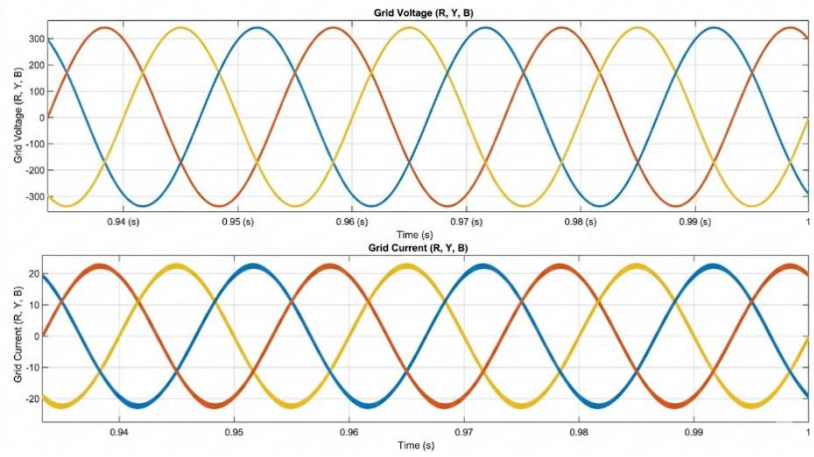

Figure 23. Three phase grid voltages and current in G2V mode

4.3. Total harmonic distortion in single battery vehicle-to-grid and grid-to-vehicle operation

Figures 24(a) and (b) illustrate the FFT analysis and corresponding %THD of the grid current without and with the traditional controller, respectively. Figure 24(c) presents the FFT analysis of the proposed method, where the %THD is reduced to 2.39% in the MATLAB FFT window. This value is significantly lower than the IEEE standard limit of 5% (519–1992), demonstrating the improved harmonic performance of the proposed controller.

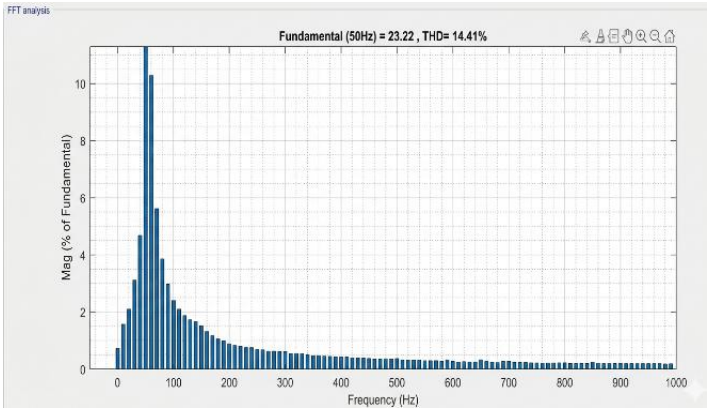

(a)

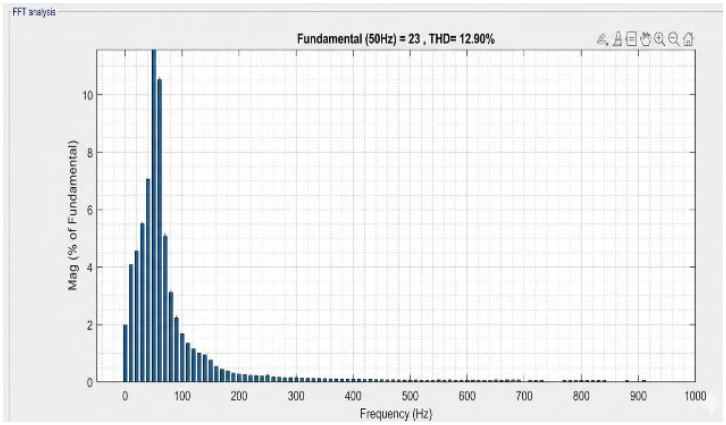

(b)

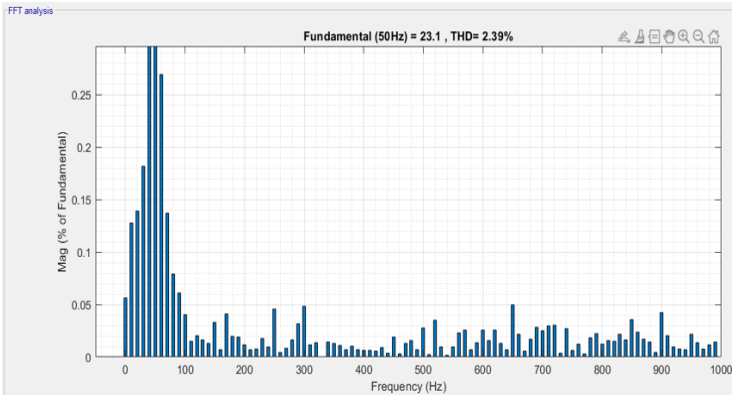

(c)

Figure 24. FFT window of single battery V2G and G2V operation (a) %THD without dq-PI controller, (b) %THD with Mdq-PI controller, and (c) %THD with MDq controller

Table 5 depicts the comparative performance of traditional and proposed control strategy in improving performance of the design by reducing harmonic distortion to provide quality power supply to the load. It clearly present proposed methodology dominance over traditional techniques by achieving 2.39% of THD with in standards.

Table 5. Performance comparison in terms of % THD and PF

Terms	PI	Mdq-PI	Proposed MDq PI
P F	0.88	0.98	0.98
	%THD		
Source current I_s	14.41	12.90	2.39

5. CONCLUSION

This research introduced a MDq control technique for a bidirectional EV charging system in V2G and G2V modes. To test system performance under actual grid settings, MATLAB/Simulink was used to simulate an EV battery, bidirectional DC–DC converter, grid-connected voltage source inverter, and LCL filter. The MDq controller outperforms conventional PI and MDq-PI controllers in power quality and dynamic performance, with grid current THD reduced to 2.39%, stable DC-link voltage regulation, near-unity power factor, and faster transient response during bidirectional power flow.

The proposed approach integrates multi-objective optimization into controller design to minimize harmonic distortion, voltage deviation, current ripple, and settling time, surpassing previous studies that used fixed-gain PI or heuristic dq-based controllers. While previous studies have improved individual performance metrics, this study shows that PSO-based tuning of the modified dq controller provides a balanced and robust solution for V2G and G2V operation, addressing key limitations in recent bidirectional charging literature. The findings confirm that optimized intelligent control significantly enhances grid stability and power quality in EV-integrated smart grids, contributing to more reliable and scalable bidirectional charging infrastructures. Future work will focus on experimental validation using a hardware prototype, extension to multi-EV charging stations, real-time implementation, and integration with renewable energy sources and higher-level energy management systems to further assess the practical applicability of the proposed control strategy.

FUNDING INFORMATION

This research was supported by Koneru Lakshmaiah Education Foundation SERB, DST (EEQ/2023/000744).

AUTHOR CONTRIBUTIONS STATEMENT

This journal uses the Contributor Roles Taxonomy (CRediT) to recognize individual author contributions, reduce authorship disputes, and facilitate collaboration.

Name of Author	C	M	So	Va	Fo	I	R	D	O	E	Vi	Su	P	Fu
Devarakonda Balasubramanyam	✓	✓	✓	✓	✓	✓		✓	✓	✓			✓	
Goda Ganesh Raja Sekhar		✓				✓		✓	✓	✓	✓	✓		
Tadanki Vijay Muni	✓		✓	✓		✓	✓			✓	✓		✓	✓

C : **C**onceptualization
M : **M**ethodology
So : **So**ftware
Va : **Va**lidation
Fo : **Fo**rmal analysis
I : **I**nvestigation
R : **R**esources
D : **D**ata Curation
O : Writing - **O**riginal Draft
E : Writing - Review & **E**diting
Vi : **Vi**sualization
Su : **Su**pervision
P : **P**roject administration
Fu : **Fu**nding acquisition

CONFLICT OF INTEREST STATEMENT

Authors state no conflict of interest.

DATA AVAILABILITY

Data availability is not applicable to this paper as no new data were created or analyzed in this study.

REFERENCES

[1] S. Penagaluru and T. G. Manohar, "Review on renewable source integrated topologies with power quality enhancing strategies," *International Journal of Renewable Energy Research*, vol. 8, no. 4, pp. 2350–2366, 2018, doi: 10.20508/ijrer.v8i4.8659.g7537.

[2] K. Sudheer, P. Suresh, R. Sireesha, and K. Yamuna, "COVID-19 Propagation Unified Controller for Improved Power Quality in Multi Feeder Renewable Integrated System," *Przeglad Elektrotechniczny*, vol. 1, no. 6, pp. 116–121, Jun. 2024, doi: 10.15199/48.2024.06.22.

[3] Z. Zhang, B. Liu, and S. Song, "Power Decoupling Control for V2G/G2V/PV2G Operation Modes in Single-Phase PV/Battery Hybrid Energy System with Low DC-Link Capacitance," *IEEE Access*, vol. 9, pp. 160975–160986, 2021, doi: 10.1109/ACCESS.2021.3131626.

[4] M. A. Islam *et al.*, "Modeling and Performance Evaluation of ANFIS Controller-Based Bidirectional Power Management Scheme

in Plug-In Electric Vehicles Integrated with Electric Grid," *IEEE Access*, vol. 9, pp. 166762–166780, 2021, doi: 10.1109/ACCESS.2021.3135190.
[5] B. Chelladurai, C. K. Sundarabalan, S. N. Santhanam, and J. M. Guerrero, "Interval Type-2 Fuzzy Logic Controlled Shunt Converter Coupled Novel High-Quality Charging Scheme for Electric Vehicles," *IEEE Transactions on Industrial Informatics*, vol. 17, no. 9, pp. 6084–6093, Sep. 2021, doi: 10.1109/TII.2020.3024071.
[6] A. K. Seth and M. Singh, "Second-Order Ripple Minimization in Single-Phase Single-Stage Onboard PEV Charger," *IEEE Transactions on Transportation Electrification*, vol. 7, no. 3, pp. 1186–1195, Sep. 2021, doi: 10.1109/TTE.2021.3049559.
[7] H. C. Chen and B. W. Huang, "Integrated G2V/V2G Switched Reluctance Motor Drive with Sensing only Switch-Bus Current," *IEEE Transactions on Power Electronics*, vol. 36, no. 8, pp. 9372–9381, Aug. 2021, doi: 10.1109/TPEL.2021.3054875.
[8] P. Inampudi, P. Chandrasekar, and T. V. Muni, "Evaluating a novel bidirectional soft-switching DC-DC converter for electric vehicles," *International Journal of Applied Power Engineering*, vol. 13, no. 4, pp. 825–834, Dec. 2024, doi: 10.11591/ijape.v13.i4.pp825-834.
[9] S. H. Hosseini, R. Ghazi, and H. Heydari-Doostabad, "An Extendable Quadratic Bidirectional DC-DC Converter for V2G and G2V Applications," *IEEE Transactions on Industrial Electronics*, vol. 68, no. 6, pp. 4859–4869, Jun. 2021, doi: 10.1109/TIE.2020.2992967.
[10] A. Verma and B. Singh, "AFF-SOGI-DRC Control of Renewable Energy Based Grid Interactive Charging Station for EV with Power Quality Improvement," *IEEE Transactions on Industry Applications*, vol. 57, no. 1, pp. 588–597, Jan. 2021, doi: 10.1109/TIA.2020.3029547.
[11] J. J. Kao, C. L. Lin, Y. C. Liu, C. C. Huang, and H. S. Jian, "Adaptive Bidirectional Inductive Power and Data Transmission System," *IEEE Transactions on Power Electronics*, vol. 36, no. 7, pp. 7550–7563, Jul. 2021, doi: 10.1109/TPEL.2020.3047069.
[12] H. Heydari-Doostabad and T. O'Donnell, "A Wide-Range High-Voltage-Gain Bidirectional DC-DC Converter for V2G and G2V Hybrid EV Charger," *IEEE Transactions on Industrial Electronics*, vol. 69, no. 5, pp. 4718–4729, May 2022, doi: 10.1109/TIE.2021.3084181.
[13] K. P. Inala, B. Sah, P. Kumar, and S. K. Bose, "Impact of V2G Communication on Grid Node Voltage at Charging Station in a Smart Grid Scenario," *IEEE Systems Journal*, vol. 15, no. 3, pp. 3749–3758, Sep. 2020, doi: 10.1109/jsyst.2020.3007320.
[14] G. G. Kumar and K. Sundaramoorthy, "Dual-Input Nonisolated DC-DC Converter With Vehicle-to-Grid Feature," *IEEE Journal of Emerging and Selected Topics in Power Electronics*, vol. 10, no. 3, pp. 3324–3336, Jun. 2022, doi: 10.1109/JESTPE.2020.3042967.
[15] K. Sudheer and R. Sudha, "Enhancement of Power Quality in Multi Feeder Three Phase System with Photovoltaic fed ANFIS-Unified Multi Converter Controller," in *MATEC Web of Conferences*, vol. 225, p. 03015, Nov. 2018, doi: 10.1051/matecconf/201822503015.
[16] S. Taghizadeh, M. J. Hossain, N. Poursafar, J. Lu, and G. Konstantinou, "A Multifunctional Single-Phase EV On-Board Charger with a New V2V Charging Assistance Capability," *IEEE Access*, vol. 8, pp. 116812–116823, 2020, doi: 10.1109/ACCESS.2020.3004931.
[17] P. K. Inampudi, C. Perumal, V. R. Guntreddi, and T. V. Muni, "A Novel DC-DC Boost Converter with Coupled Inductors for High Gain and Smooth Switching," *Journal of Advanced Research in Applied Sciences and Engineering Technology*, vol. 48, no. 2, pp. 92–104, Jul. 2025, doi: 10.37934/araset.48.2.92104.
[18] S. Liu, D. Xin, L. Yang, J. Li, and L. Wang, "A hierarchical V2G/G2V energy management system for electric-drive-reconstructed onboard converter," *IEEE Access*, vol. 8, pp. 198201–198213, 2020, doi: 10.1109/ACCESS.2020.3034968.
[19] N. M. Razali, H. Mohamad, A. F. Abidin, and Z. Ali, "a Hybrid Mvo-Bmo Technique for Plug-in Electric Vehicle Charging Optimization," *Jurnal Teknologi*, vol. 86, no. 5, pp. 23–34, Aug. 2024, doi: 10.11113/jurnalteknologi.v86.20625.
[20] A. Dixit, P. Swarnkar, and R. K. Nema, "Grid Integrated Bidirectional EV Battery Charger in V2G-G2V Mode With Improved Power Quality," in *2023 IEEE International Students' Conference on Electrical, Electronics and Computer Science, SCEECS 2023*, Feb. 2023, pp. 1–6, doi: 10.1109/SCEECS57921.2023.10062990.
[21] R. Rana, T. S. Saggu, S. S. Letha, and F. I. Bakhsh, "V2G based bidirectional EV charger topologies and its control techniques: a review," *Discover Applied Sciences*, vol. 6, no. 11, p. 588, Nov. 2024, doi: 10.1007/s42452-024-06297-z.
[22] F. Justin, G. Peter, A. A. Stonier, and V. Ganji, "Power Quality Improvement for Vehicle-to-Grid and Grid-to-Vehicle Technology in a Microgrid," *International Transactions on Electrical Energy Systems*, vol. 2022, pp. 1–17, Aug. 2022, doi: 10.1155/2022/2409188.
[23] N. K. K., J. N. S., and V. K. Jadoun, "A combined approach to evaluate power quality and grid dependency by solar photovoltaic based electric vehicle charging station using hybrid optimization," *Journal of Energy Storage*, vol. 84, p. 110967, Apr. 2024, doi: 10.1016/j.est.2024.110967.
[24] G. Srihari, R. S. R. K. Naidu, P. Falkowski-Gilski, P. B. Divakarachari, and R. K. V. Penmatsa, "Integration of electric vehicle into smart grid: a meta heuristic algorithm for energy management between V2G and G2V," *Frontiers in Energy Research*, vol. 12, Apr. 2024, doi: 10.3389/fenrg.2024.1357863.
[25] M. Costa and G. Del Papa, "Digital Twins for Intelligent Vehicle-to-Grid Systems: A Multi-Physics EV Model for AI-Based Energy Management," *Applied Sciences (Switzerland)*, vol. 15, no. 15, p. 8214, Jul. 2025, doi: 10.3390/app15158214.

BIOGRAPHIES OF AUTHORS

Devarakonda Balasubramanyam is an Associate Professor who began his academic career in 2010 at Siddartha Educational Academy Group of Institutions and currently serves as Head of the Department. He has broad teaching experience in core power system subjects and is a research scholar at KL University. His research focuses on power systems, smart grids, and power quality improvement. He can be contacted at email: balurayofhope@gmail.com.

Goda Ganesh Raja Sekhar is an Associate Professor of Electrical and Electronics Engineering (EEE) at KL University, Vaddeswaram, with 25 years of administrative and teaching experience. His degrees are B.E. in Electrical and Electronics Engineering from Karnatak University, M.Tech. in High Voltage Engineering from JNTUH, and a Ph.D. from Acharya Nagarjuna University. Over 50 undergraduate (UG) and 10 postgraduate (PG) projects, and 2 Ph.D. scholars are under his supervision. He has published over 50 research papers (including 3 SCI-indexed and 31 Scopus-indexed papers), 6 national and international patents, and a textbook on Renewable Energy Sources. He was named Best Teacher and Visionary Edu-Leader of the Year 2023. International publications and conferences employ him as a reviewer, editor, and editorial board member. Power systems, high voltage engineering, system operation and control, and renewable energy are his research areas. He has 12 professional memberships, 10 online certification courses, and is a Senior Member of IEEE and a Life Member of ISTE member. He can be contacted at email: rsgg73@gmail.com or rsgg73@kluniversity.in.

Tadanki Vijay Muni is an Assistant Professor and researcher with more than 14 years of experience in the Department of Electrical and Electronics Engineering at KL Deemed to be University. He received his B.Tech. degree in Electrical and Electronics Engineering from JNTU Hyderabad, an M.Tech. degree in Power and Industrial Drives from JNTUK, Kakinada, and doctoral degree from KL Deemed to be University. He has authored 6 textbooks on electrical discipline. He has published over 62 Scopus-indexed publications, 15 Web of Science-indexed articles, 15 peer-reviewed articles, and 6 patents with two grants. He studies power electronic converters, energy management systems, power grid control, renewable energy, and microgrids. He is an active Senior Member of IEEE. He can be contacted at email: vijaymuni1986@gmail.com.